

Research Paper

# Diallyl Trisulfide Inhibits Growth of NCI-H460 *in Vitro* and *in Vivo*, and Ameliorates Cisplatin-Induced Oxidative Injury in the Treatment of Lung Carcinoma in Xenograft Mice

Xiaoyan Jiang<sup>1</sup>, Xiaosong Zhu<sup>1</sup>, Na Liu<sup>1</sup>, Hongya Xu<sup>1</sup>, Zhongxi Zhao<sup>1,2,3</sup>✉, Siying Li<sup>1</sup>✉, Shanzhong Li<sup>3</sup>, Jianhua Cai<sup>3</sup> and Jimin Cao<sup>3</sup>

1. School of Pharmaceutical Sciences, Shandong University, 44 West Wenhua Road, Jinan, Shandong 250012, P.R. China.

2. Shandong Provincial Key Laboratory of Mucosal and Transdermal Drug Delivery Technologies, Shandong Academy of Pharmaceutical Sciences, 989 Xinluo Street, Jinan, Shandong 250101, P.R. China.

3. Jiangsu Shengshi Kangde Biotech Corporation, Lianyungang, Jiangsu 222006, P.R. China.

✉ Corresponding authors: Professor Zhongxi Zhao, Tel: +86-531-88382187; Fax: +86-531-88382548. E-mail: zxzhaosdu.edu.cn or usxzhaogmail.com. Siying Li, E-mail: li-siying@hotmail.com.

© Ivyspring International Publisher. This is an open access article distributed under the terms of the Creative Commons Attribution (CC BY-NC) license (<https://creativecommons.org/licenses/by-nc/4.0/>). See <http://ivyspring.com/terms> for full terms and conditions.

Received: 2016.07.13; Accepted: 2016.09.06; Published: 2017.01.15

## Abstract

Diallyl trisulfide (DATS), an organosulfuric component of garlic oil, exhibits potential anticancer and chemopreventive effects. Cisplatin (DDP), a common chemotherapeutic agent, has provided great therapeutic contributions to treating solid tumors, but with serious side effects. Here, we verified the anti-tumor properties of DATS on lung cancer *in vitro* and *in vivo*, and evaluated synergistic effects of DATS combined with DDP on the NCI-H460 xenograft model. Significantly decreased cell viabilities, cell cycle G<sub>1</sub> arrest, and apoptosis induction were observed in DATS treated NCI-H460 cells ( $p < 0.05$ ). And injection of DATS (30 or 40 mg/kg) to female Balb/c mice significantly inhibited the growth of human NCI-H460 cell tumor xenograft ( $p < 0.001$ ). Moreover, DATS in combination with DDP exhibited enhanced anti-tumor activity via induction of apoptosis. Apoptosis pathways were confirmed by modulation of p53, Bcl-2 family members; induction of active caspase-3/8/9 and activation of JNK- and p38-MAPK pathways. Interestingly, DATS+DDP administration exerted fewer side effects, such as suppressing the weight loss and ameliorating DDP-induced oxidative injury, especially in renal parenchyma. In addition, increased E-cadherin and decreased MMP-9 expression levels were observed in DATS-treated tumor tissues. These studies provide supports that DATS might be a potential candidate for combination with DDP in cancer treatment.

Key words: Diallyl trisulfide; cisplatin; lung carcinoma; enhanced effect; attenuate side effect.

## Introduction

Lung cancer is one of the most common causes of cancer death, while recent decades have witnessed the efforts in improving the treatment of lung cancer via surgical therapies and adjuvant chemotherapy. However, strong side effects, such as serious damages on normal organs, often occur and lead to cessation of treatment, which already has been a bottleneck in current cancer treatment. For example, Cisplatin (DDP), as a common chemotherapeutic agent, has

provided great therapeutic contributions to lung cancer treatment. But nephrotoxicity induced by oxidative stress, the major clinical side effect of DDP, limits its wide application of cancer treatment [1]. Therefore, it is necessary to develop adjuvants from natural bioactives that are safe and do not influence treatment effects.

Medicinal plants and natural herbal products are often administered in combination with

chemotherapeutic drugs to increase their potential antioxidant activity and provide better protections against their nephrotoxic effects. Garlic (*Allium sativum*) has long been used both for flavoring and for the potential benefits of preventing and curing ailments in many cultures. Epidemiologic evidence showed that the raw garlic consumption was associated with reduced risk of lung cancer in a Chinese population [2, 3]. Organosulfur compounds (OSCs) were known to be the major active components of garlic, including diallyl sulfide (DAS), diallyl disulfide (DADS), diallyl trisulfide (DATS), methylallyl disulfide, methylallyl trisulfide, ajoenes, etc [4]. Among them, DATS has been synthesized chemically and extensively consumed in China for several years and has been used as the major active constituent of garlic dietary supplements. In the drug metabolism and pharmacokinetics study, DADS was observed in rat plasma after a jugular vein cannula administration of DATS [5]. And in another report, allyl mercaptan (AM) and allyl methyl sulfide (AMS), allyl methyl sulfoxide (AMSO) and allyl methyl sulfone (AMSO<sub>2</sub>) were identified as DADS metabolites with a long-circulating characteristic in the stomach, plasma, liver and urine of rats [6], which suggested that DATS might behave like prodrug and its active metabolites could provide mechanistic evidences for multiple targets in physiological systems. Besides, it had been documented that the number of sulfur atom and allyl group in allylsulfides were important factors to determine the chemical and biological activities of garlic-derived organosulfides [7, 8]. Based on these results, we choose DATS as a target compound.

To date, many studies suggested that DATS had multiple health benefits, such as anti-cancer, anti-inflammation and immunomodulation [9]. In cancer chemoprevention, DATS decreased the carcinogen-induced cancers in experimental animals and inhibited the proliferation of various types of cancer cells. Its mechanisms might be relevant with cell cycle arrest, induction of apoptotic cell death, suppression of oncogenic signal transduction pathways and inhibition of cell invasion [10]. Besides, DATS exerted protection action in some damage model, such as neuroprotection against oxygen glucose deprivation-induced neural cell injury [11], anti-inflammatory effect in mouse paw edema induced by LPS [12], protection against high glucose-triggered oxidative stress in H9c2 cardiomyoblast cells [13], etc. Furthermore, there were evidences that aged garlic extract (or garlic) acted as an immune booster by enhancing lymphocyte proliferation, macrophage phagocytosis, macrophage and lymphocyte infiltration into tumor, as well as

releasing cytokines [14-16].

Despite these inspiring results for cancer treatments, organosulfur compounds have the disadvantage of low bioavailability which discounts their anti-cancer effect. Therefore, they often combine with other agents to exert synergistic effects or ameliorate side effects. For example, co-administration of aged garlic extract (AGE) with Naltrexone resulted in improvement of immune responses against implanted fibrosarcoma tumors in BAL b/c mice [17]. AGE pretreatment not only exerted the cardioprotective effect against Doxorubicin-induced cardiotoxicity, but also increased the Doxorubicin uptake into tumor cells and increased the long term survivors of tumor-bearing mice [18]. A biochemical study showed that co-administration of garlic extract and Metformin also had curative and protective activities against Gentamicin nephrotoxicity in Wistar rats [19].

Based on these results, we carried out these studies to verify the possible therapeutic effect of DATS on human lung cancer *in vitro* and *in vivo*. Besides, we investigated whether DATS combined with DDP exerted enhanced anticancer activity, meanwhile, attenuated DDP-induced side effects.

## Materials and Methods

### Materials and reagents

Diallyl trisulfide (DATS, 98 %) was obtained from AIKE Regent (Chengdu, China). Sulforhodamine B (SRB), 4',6-diamidino-2-phenylindole (DAPI) and propidium iodide (PI) were purchased from Sigma-Aldrich (St. Louis, Missouri, USA). Primary antibodies against p21, p53, Bax, Bcl-2, Bcl-xl, Cytochrome C, CyclinA2, CyclinB1, CyclinD1, CyclinE1, MMP-9, PCNA and FADD were obtained from Abcam (Cambridge, United Kingdom). The antibodies against caspase-3/7/8/9, cleaved caspase-3/7/8/9, cleaved PARP, ERK, p-ERK, JNK, p-JNK, p38, p-p38 were from Cell Signaling Technology (Danver, MA, USA). Nrf2, AKT, p-AKT antibodies were from Santa Cruz Technology, Inc. (Heidelberg, Germany) and anti-E-cadherin antibody was from Millipore (Bedford, MA, USA). Other reagents were purchased from Sigma-Aldrich (St. Louis, Missouri, USA).

### Cell lines and cell culture

The human lung carcinoma cell line (NCI-H460) was purchased from Chinese Academy of Sciences Cell Bank (Shanghai China). The cell line was cultured in RPMI-1640 (GIBCO, USA) supplemented with 10 % fetal bovine serum (BI, Australia), 1 % penicillin-streptomycin at 37 °C in a humidified incubator of 5 % CO<sub>2</sub>. When the growing cells reached

approximately 70-90 % confluence, they were treated with diallyl trisulfide.

### Determination of cell viability by SRB assay

The effect of DATS on NCI-H460 cell viability was performed by SRB assay. Cells at a density of  $5 \times 10^3$  cells were grown on 96-well cell culture plates for 12 h and exposed to different concentrations of DATS (25, 50, 100, 200, 400  $\mu\text{M}$ ) for 24, 48 and 72 h. After treatment, cells were fixed with 10 % trichloroacetic acid (TCA) for 1 h at 4 °C. Then each well was added with 100  $\mu\text{L}$  of SRB solution (0.4 % w/v), and incubated at room temperature for 30 min. And then, the supernatant were removed and re-suspended with 200  $\mu\text{L}$  of 10 mM un-buffered Tris Base (pH 10.5) to dissolve the pink crystals, and the absorbance was detected at 540 nm using Microplate Reader (Safire2, TECAN, France). All experiments were performed in triplicate.

### Cell cycle analysis by Flow Cytometry

Effect of DATS on cell cycle distribution of NCI-H460 cells was analyzed by flow cytometry. The NCI-H460 cells were grown on 6 well plates and grown overnight to achieve 80 % confluence. After treatment with DATS (0, 50, 100, 200  $\mu\text{M}$ ), all the cells were harvested, fixed with iced 70 % ethanol at -20 °C overnight, centrifuged and incubated with 0.5 mL of PBS containing 100  $\mu\text{g}/\text{mL}$  RNase for 30 min at 37 °C, and then incubated with 50  $\mu\text{g}/\text{mL}$  PI for 30 min in the dark at 4 °C. The cellular DNA content was analyzed by a Beckman Coulter model FC500 flow cytometer (Brea, CA, USA). A minimum of 10,000 cells per sample were counted and DNA histograms were analyzed by using MODFIT software (Verity Software House, Topsham, Maine, USA).

### DAPI staining

Apoptosis-inducing effect of DATS on NCI-H460 cells was analyzed by DAPI staining. In brief, the NCI-H460 cell was grown on 24-well plates and treated with DATS (0, 50, 100  $\mu\text{M}$ ) for 24 h. The cellular monolayer was fixed with cold methanol/acetone (1:1) and stained with DAPI solution. The morphological features of apoptosis (cell shrinkage, chromatin condensation, and fragmentation) were monitored by fluorescence microscopy (Olympus IX 71, Tokyo, Japan).

### Apoptosis analysis by Annexin V and Propidium iodide

For quantitative analysis of apoptosis, the NCI-H460 cells were analyzed by Annexin V-FITC/PI Apoptosis Detection Kit (Invitrogen, Carlsbad, USA). In brief, the NCI-H460 cell was grown on 6 well-plates and treated with DATS (50, 100, 200  $\mu\text{M}$ ) for 24 h.

Detached and adherent cells were harvested and washed with PBS, then re-suspended in the binding buffer and stained with Annexin V and propidium iodide (PI) according to the manufacturers' instructions. Apoptotic cells were analyzed by a Beckman Coulter model FC500 flow cytometer (Brea, CA, USA).

### Animal and tumor xenograft model

Xenograft model of gastric cancer was established by a subcutaneous injection (s.c.) of  $3 \times 10^6$  NCI-H460 cells into six-week-old female BAL b/c nude mice (Institute of Laboratory Animal Sciences, Cams&Pumc; Beijing, China). Following two weeks of growth, tumor tissues were cut into multiple  $2 \times 2 \times 2$  mm<sup>3</sup> pieces and implanted (s.c.) into the left fore armpit of each mouse using a range trocar. Tumor diameters were measured with a caliper and tumor volume was calculated by the formula: (width)<sup>2</sup> × length/2. Treatments were started after one week when the tumors reached an average volume of 100–200 mm<sup>3</sup>. Animals were randomly divided into 7 groups (n = 7) and intraperitoneally injected with: (a) HP- $\beta$ -CD; (b) 20 mg/kg DATS; (c) 30 mg/kg DATS; (d) 40 mg/kg DATS; (e) 4 mg/kg DDP; (f) 4 mg/kg DDP + 20 mg/kg DATS; (g) 4 mg/kg DDP + 30 mg/kg DATS. HP- $\beta$ -CD and DATS were administrated every day and DDP was administrated once 5 days. After 24 days of treatment, mice were sacrificed; tumors and major tissues were weighed and excised for histopathological analysis. Tissues index was calculated by the following formula:  $[\text{Weight}_{(\text{tissue})} / \text{Weight}_{(\text{body})}] \times 10$  g. The antitumor activity of DATS was calculated as a T/C (% of control for growth). T/C was calculated according to the formula:  $(T/C) \times 100\%$ . T and C are the changes in tumor volume ( $\Delta\text{growth}$ ) for the treated and vehicle/control groups, respectively. All procedures were approved by the Ethical committee of school of Medicine, Shandong University, China.

### Hematoxylin and Eosin (HE) and Immunohistochemistry

Tumor tissues were formalin-fixed, paraffin-embedded and sectioned at 4  $\mu\text{m}$ . Afterwards, the tissue section was deparaffinized and rehydrated. To visualize histology and to check for live and dead cells, the tissue sections were stained with hematoxylin and eosin (H&E). To further evaluate apoptotic/necrotic and mitotic cells, the apoptotic fraction of the tumors was shown by staining with bax, p21, p53 and Ki67 antibody. Binding of primary antibodies was detected with horseradish peroxidase-conjugated secondary antibody. Signals were visualized by

diaminobenzidine reaction and counterstained with hematoxylin.

### Detection of apoptotic cells in situ

TdT-mediated dUTP nick end labeling (TUNEL) was performed with an apoptosis detection kit (Roche, California, USA) according to the manufacturer's instructions. In brief, tissue sections were deparaffinized, rehydrated through a graded alcohol series, and rinsed in distilled water. The tissue sections were incubated with proteinase K for 20 min at room temperature and subsequently incubated with equilibration buffer and terminal deoxynucleotidyl transferase (TdT) enzyme in a humidified chamber for 1 h at 37 °C. Finally, sections were incubated with antidigoxigenin -peroxidase conjugate. Tissue peroxidase activity was evaluated through DAB application. Cells undergoing apoptosis contained dark brown staining nuclei.

### Western blot analysis

The NCI-H460 cells were seeded in 6 cm plastic dishes and incubated with different concentrate of DATS (0, 50, 100, 200  $\mu$ M) for 48 h. After that, the cells were washed with PBS and lysed with RIPA cell lysis buffer containing a protease inhibitor cocktail. Tumors tissues from representative mice were homogenated and lysed for western blotting analysis. These samples were then centrifuged at 12,000 g for 15 min at 4 °C. The supernatants were collected and the protein levels were determined by BCA protein assay kit (Beijing Solarbio Science & Technology Co., Ltd. China) with bovin serum albumin (BSA) as a standard. Total proteins (50  $\mu$ g/lane) were separated by 8-15 % SDS-PAGE, and transferred on a polyvinylidene difluoride membrane (PVDF, Immobilon-P Transfer Membrane, Millipore). The membranes were blocked in 5 % skim milk for 2 h at room temperature, and then probed with the appropriate primary antibodies (1:1000) at 4 °C overnight. After washing, membranes were incubated with horseradish-peroxidase (HRP) -conjugated secondary antibody (1:10000) in TBST containing 5 % milk at room temperature for 2 h. Then, the membrane preparations were washed three times in TBST and visualized by enhanced chemiluminescence system (Merck Millipore, Darmstadt, Germany). The films were subsequently scanned, and the signal intensity of each band was determined by Alphamager HP system (Cell Biosciences, Inc., Santa Clara, CA, USA).

### Statistical analysis

Results were given as means  $\pm$  standard deviation (SD) or means  $\pm$  standard error (SEM). Student's t test analysis and analysis of variance

(ANOVA) were used to analyze differences between treatment and control groups. The curves and histograms were drawn by Graphpad prime 6.0 software. Statistical significance was determined as \* $p$  < 0.05, \*\*  $p$  < 0.01 or \*\*\* $p$  < 0.001.

## Results

### DATS suppressed cell growth and induced cell cycle arrest in NCI-H460 cells

We evaluated the *in vitro* anti-proliferative activities of DATS on human lung cancer NCI-H460 cells by SRB assay. Results showed that DATS has a significant inhibition in growth of NCI-H460 cells with a time- and dose- dependent manner (Fig 1A). The IC<sub>50</sub> value of DATS was 130.3, 37.5 and 18.5  $\mu$ M (for 24, 48 and 72 h respectively). Based on these results, we evaluated cell cycle distribution change affected by DATS at 50, 100 and 200  $\mu$ M concentrations for 24 h treatment by flow cytometer analysis. As shown in Fig 1B, high dose of DATS treatment (200  $\mu$ M) induced an accumulation of cells in the G<sub>0</sub>/G<sub>1</sub> phase and a corresponding decrease in S phase fraction in NCI-H460 cells. Cell cycle progression is driven by heterodimeric complexes formed by cyclin D, cyclin E, cyclin A or cyclin B with cyclin-dependent kinase 4 (CDK4), CDK6, CDK2 or CDK1 [20]. To further characterize these alterations in cell cycle distribution, changes in the cyclin expression patterns were analyzed by Western blotting (Fig 1D). The DATS-induced G<sub>0</sub>/G<sub>1</sub>-phase increase and the respective loss of cells in S phase correlated well with an increase in protein levels of cyclin D1 and E1. In parallel, loss of cells in G<sub>2</sub>/M phase was indicated by reduction of the G<sub>2</sub>/M checkpoint cyclins B1 and A2 specifically at the higher DATS concentrations [21]. In addition, the accumulation of sub-G<sub>1</sub> phase cells, a hallmark of apoptosis, was noted after DATS treatment (Fig 1C). These results suggested that DATS exerted growth inhibition viability of NCI-H460 cells at least in part by induction of cell cycle arrest.

### DATS induced apoptosis in NCI-H460 cells

Based on the facts that an obvious apoptosis peak appears in cell cycle analysis, we investigated the effect of DATS on apoptosis induction in NCI-H460 cells. DAPI staining was used to analyze the morphological changes of cells treated with DATS. Some characteristic of apoptotic cell death, such as fragmented chromatin, nuclear construction loss and apoptotic bodies formation was observed as illustrated in Fig 2A. Quantification of the percentage of apoptosis induced by DATS on NCI-H460 cells was performed by Annexin V/PI staining and analyzed by

a flow cytometer. As shown in Fig 2B, DATS treatment caused significant increases in the fraction of apoptotic cells in a dose-dependent manner. At a concentration of 200  $\mu\text{M}$ , DATS increased the percentage of apoptotic cells (early and late apoptotic

cells) by over four-fold compared to the control group (Fig 2C). These results suggested DATS could efficiently induce apoptosis of NCI-H460 cells to suppress cell proliferation.

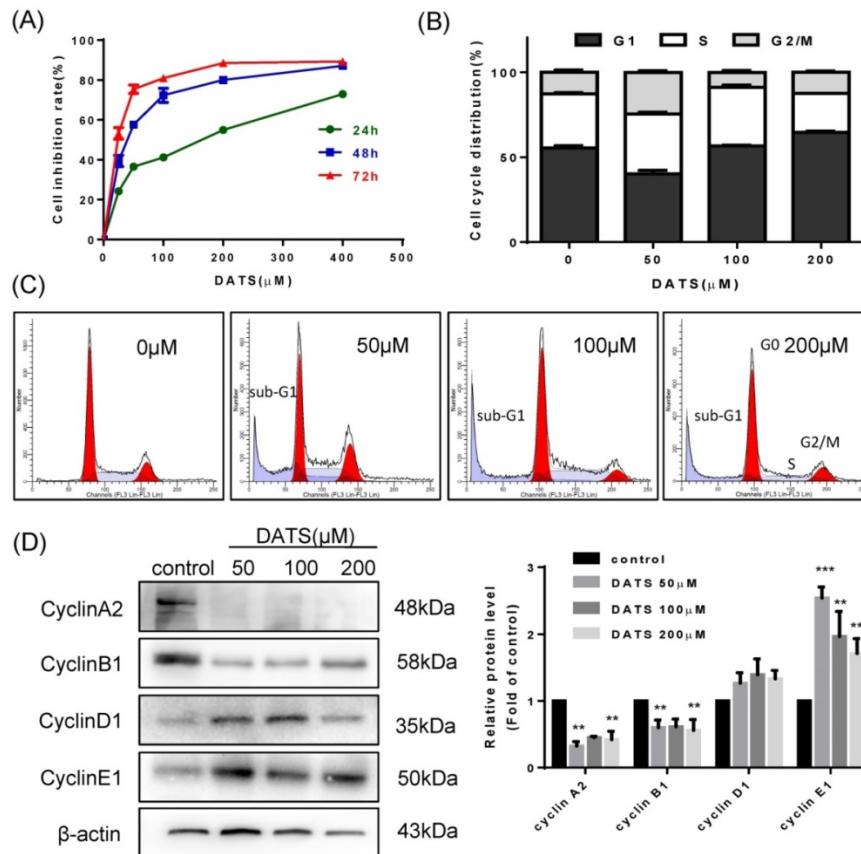


**Figure 1. DATS inhibits cell growth and induces G0/G1 phase arrest in NCI-H460 cells. (A)** Effect of DATS on cell viability. **(B and C)** Flow cytometry analysis of cell cycle distribution affected by DATS. Percentage of cells in each phase of cell cycle was estimated by Modfit software. A typical apoptosis sub-peak was observed after DATS treatment. **(D)** Western blot analysis of the level of the G0/G1-related proteins. Densitometric quantification was performed by AlphaView software. Data are presented as the mean  $\pm$  SEM. \*\* $p < 0.01$ , \*\*\* $p < 0.001$  vs. control group.

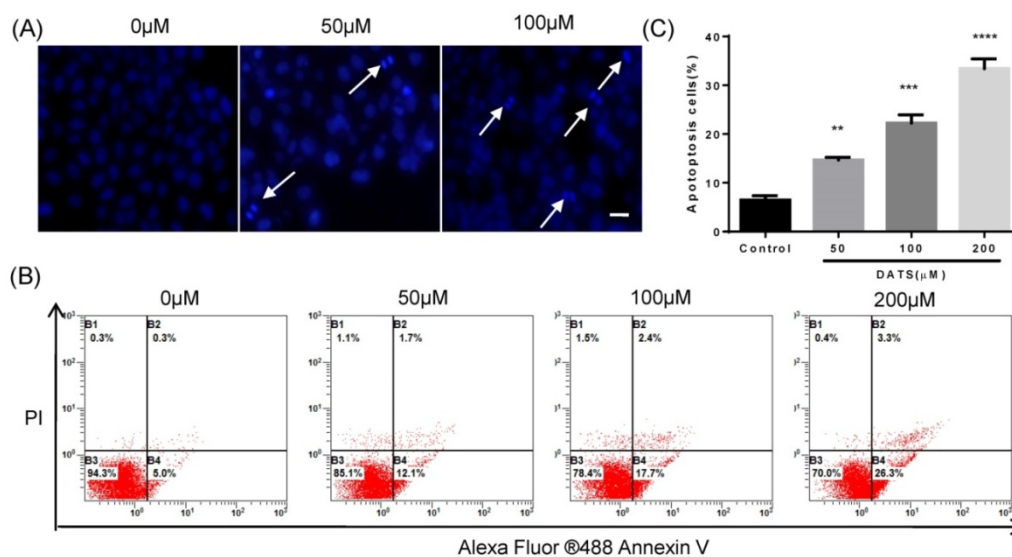


**Figure 2. DATS induced apoptosis in NCI-H460 cells. (A)** Fluorescent micrographs of DATS-treated NCI-H460 cells after DAPI staining. Scale bar = 20  $\mu\text{m}$ . **(B and C)** Flow cytometric analysis of apoptosis in NCI-H460 cells after 24 h of DATS treatment. The early and late apoptosis was quantified by CXP software. Data are presented as the mean  $\pm$  SEM. \*\* $p < 0.01$ , \*\*\* $p < 0.001$ , \*\*\*\* $p < 0.0001$  vs. control group.

### DATS induced caspases activation and regulated the repression of Bcl-2 family proteins in NCI-H460 cells

To gain more insights into the molecular mechanisms underlying the anticancer effects of DATS in NCI-H460 cells, we further investigated apoptotic related proteins by western blotting. Bcl-2 family members played a crucial role in the regulation of apoptosis [22]. Among Bcl-2 members studied, the pro-apoptotic factors bax tended to be upregulated in dose-dependent manner while the expression of pro-survival factors bcl-xL and bcl-2 were reduced after DATS treatment (Fig 3A). Furthermore, p53 and

cytochrome C were clearly generated in the DATS-treated group compared with control group.

In addition, apoptosis was precipitated by activation of cysteine proteases of caspase family, including caspase-8, 9, and 3 [23]. As shown in Fig 3B, the apoptotic cleavage of caspase-8, 9 and 3 were more pronounced in the high concentrate DATS treatment. Although we did not observed the active forms of caspase-7, DATS treatment increased the level of cleavage of PARP, which was the substrate of caspase-7 and acted as another hallmark of apoptosis. Overall, these data indicated that DATS-mediated apoptosis was essentially dependent on caspase activation and regulation Bcl-2 family proteins.

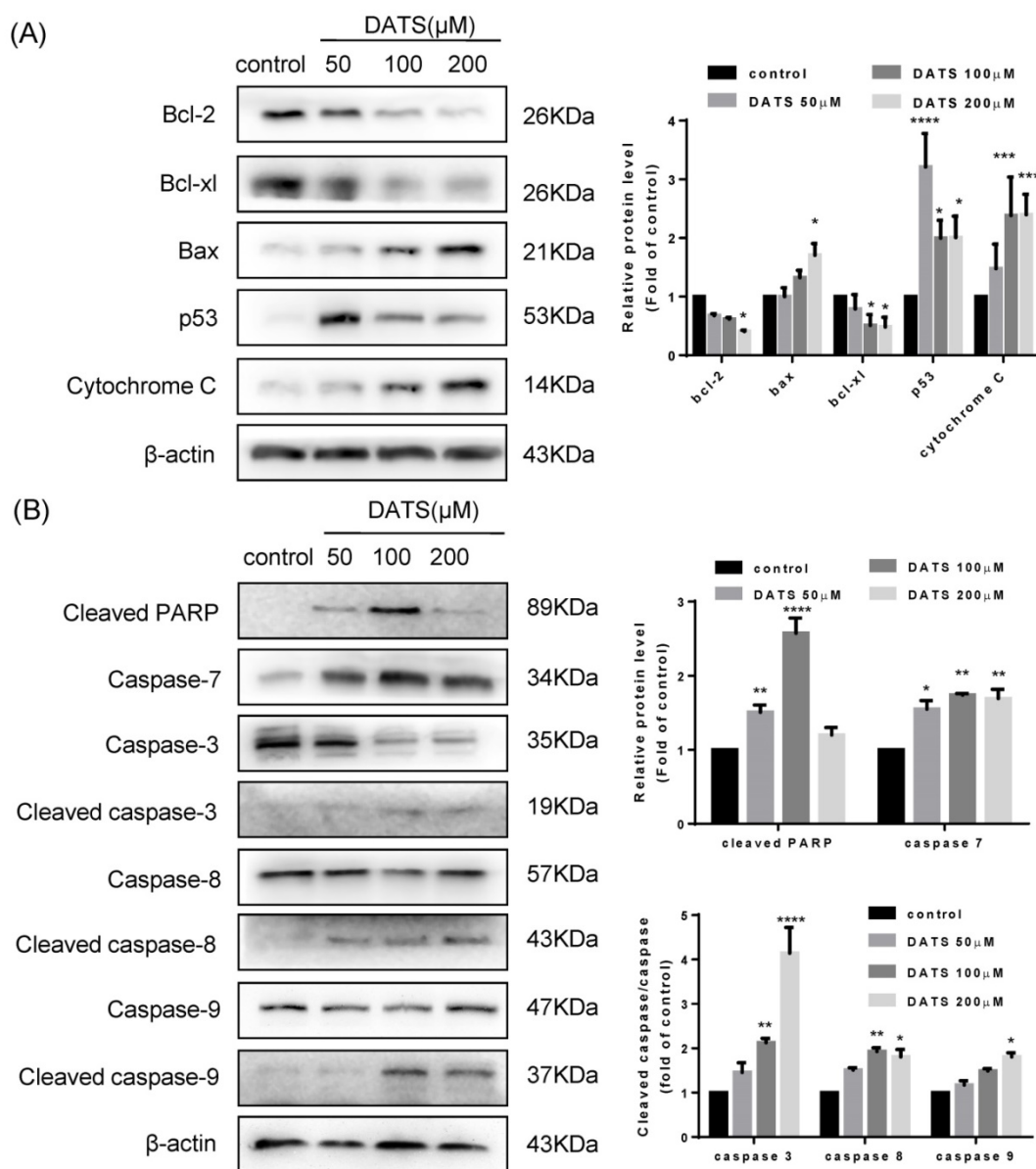


**Figure 3. Western blot analysis of the levels of the apoptosis-related protein in DATS-treated NCI-H460 cells (A) Regulation of p53, Cytochrome C and Bcl-2 family proteins (B) Activation of caspases and the degradation of PARP. Data are presented as the mean ± SEM. \*p<0.05, \*\*p<0.01, \*\*\*p<0.001 vs. control group.**

### DATS possessed anti-tumor activity and enhanced the efficacy of DDP in xenograft mice

To verify the anti-tumor activity of DATS *in vivo*, we used human lung cancer NCI-H460 tumor xenograft models. As seen in Fig 4A, DATS significantly suppressed tumor growth at doses of 30 and 40 mg/kg for 24 days compared with the control group ( $p < 0.001$  for both). In addition, there was a similar increase trend on body weight change among the control group and DATS-treated groups. Moreover, histological analysis showed no significant differences in major tissues examined (liver, kidney and spleen) (data not shown). These data showed that DATS exhibited potent anti-tumor activity and high safety *in vivo*.

We further investigated the effect of DATS in combination with DDP on NCI-H460 xenograft tumor growth in nude mice. As shown in Table 1, the mono-DDP group had a decreased tumor volume ( $846.8 \pm 161.9 \text{ mm}^3$ ) compared with the control group ( $1650.0 \pm 633.9 \text{ mm}^3$ ,  $p < 0.001$ ). The DDP+DATS (30 mg/kg) treatment showed a further decrease in the tumor volume ( $717.3 \pm 223.2 \text{ mm}^3$ ,  $p < 0.05$ ) compared with the mono-DDP therapy. Tumor-bearing mice in all groups did not show moribund conditions. Interestingly, in contrast to body weight loss of tumor-bearing mice treated with DDP alone, DATS+DDP treatment significantly reduced weight loss of mice ( $p < 0.001$ , Fig 4B). These results indicated that DATS+DDP possessed enhanced anti-tumor activity with fewer side effects in mice.

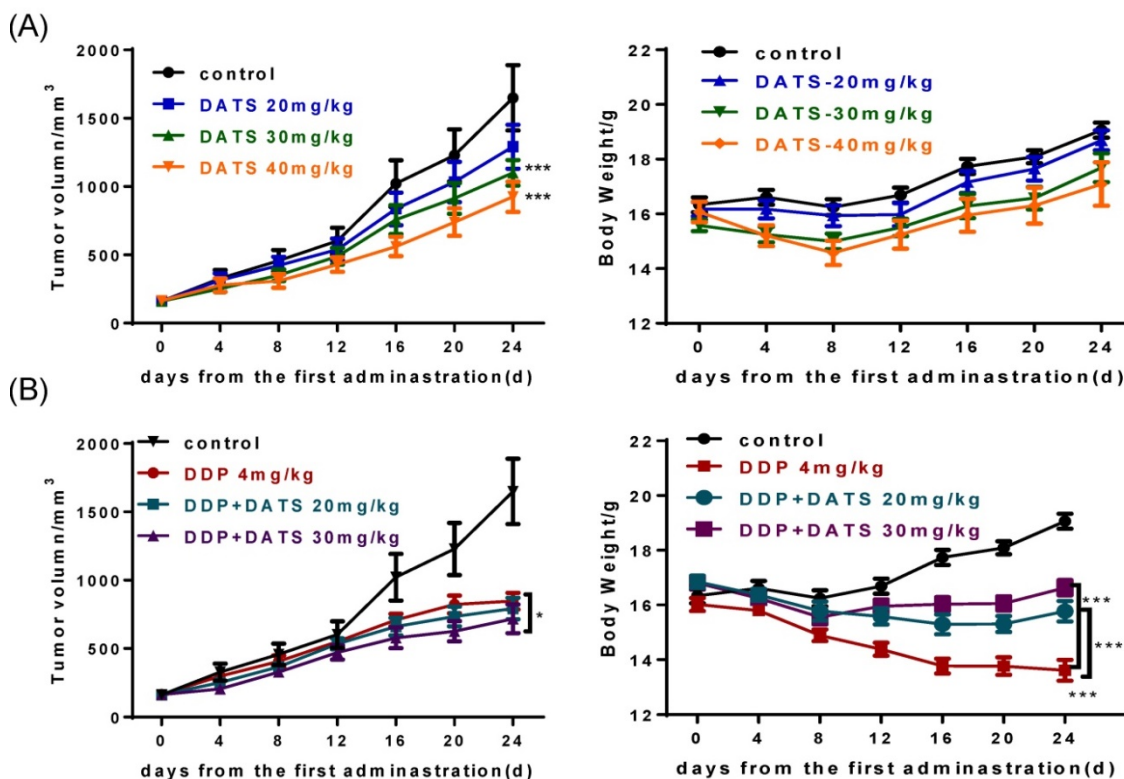


**Figure 4. DATS inhibits tumor growth and enhances the efficacy of cisplatin (DDP) in xenograft tumors.** Tumor-bearing mice (7 animals per group) were treated by intraperitoneal injection as follows: vehicle control, DATS groups (20, 30, 40 mg/kg/day), DDP (4 mg/kg/5 days) and a combination of DDP and DATS (20, 30 mg/kg) for 24 days. **(A and B)** The changes of tumor volume and body weight in DATS treatment and combination treatment groups. \* $p < 0.05$ , \*\* $p < 0.01$ , \*\*\* $p < 0.001$ .

**Table 1.** The evaluation parameter of DATS on the growth of human lung carcinoma NCI-H460 xenografts in mice (n=7).

Group	Dosage(mg/kg)	Body weight(g)	Tumor volume (mm <sup>3</sup> )	RTV	T/C(%)
Con.	vehicle	19.06±0.59/21.13±1.04	161.2±65.5/1650.0±633.9	10.80±1.33	
Pos.	DDP 4	18.23±0.56/16.44±0.95	166.3±50.7/846.8±161.9	4.94±1.23	45.7
Exp.	DATS 20	18.37±0.70/19.76±1.13	161.0±63.7/1291.9±425.8	8.21±0.75	76.0
	DATS 30	18.55±0.77/20.18±1.04	161.1±50.0/1101.3±247.6	7.06±1.25	65.4
	DATS 40	18.53±0.70/21.13±1.04	164.1±63.9/925.1±294.7	5.87±1.03	54.3
Co-treat	DDP 4+DATS 20	18.84±0.54/18.26±1.14	161.3±50.3/792.5±176.0	4.92±0.96	45.9
	DDP 4+DATS 30	18.74±0.76/19.00±1.55	163.1±44.7/717.3±223.2	4.57±0.99	42.3

### DATS inhibited tumor growth and induced apoptosis via caspase activation

H&E staining of the collected tumor samples depicted loss of cell-cell contacts and tissue disintegration in DATS-treated tumors. And DATS treatment caused marked apoptosis of tumor cells by TUNEL assay. Accordingly, we examined markers of

tumor cell proliferation (Ki67) and apoptosis (Bax, p53, p21) in NCI-H460 tumor tissues by immunohistochemistry (IHC). As shown in Fig 5A, the increased expression of p53, p21 and Bax and reduction expression of Ki67 were observed in DATS-treated tumors, which indicated the antitumor activity of DATS was correlated to reduction of tumor cell proliferation and induction of apoptosis.

Western blot analysis of xenograft tumor lysates demonstrated that DATS dramatically activated cleaved PARP by increased cleaved caspase-3 level, which was consistent with the *in vitro* findings. In addition, increased expression of FADD was also observed (Fig 5C), partially indicating that DATS-triggered apoptosis in tumor was caspase-dependent.

However, the level of proliferating cell nuclear antigen (PCNA) had no significant change after DATS treatment. Compared to DDP alone, DDP+DATS group showed a higher expression level of apoptosis markers (cleaved caspase-3 and cleaved PARP). Thus, the activity of DATS could be further boosted by co-administration of DDP in partly via increased apoptosis.

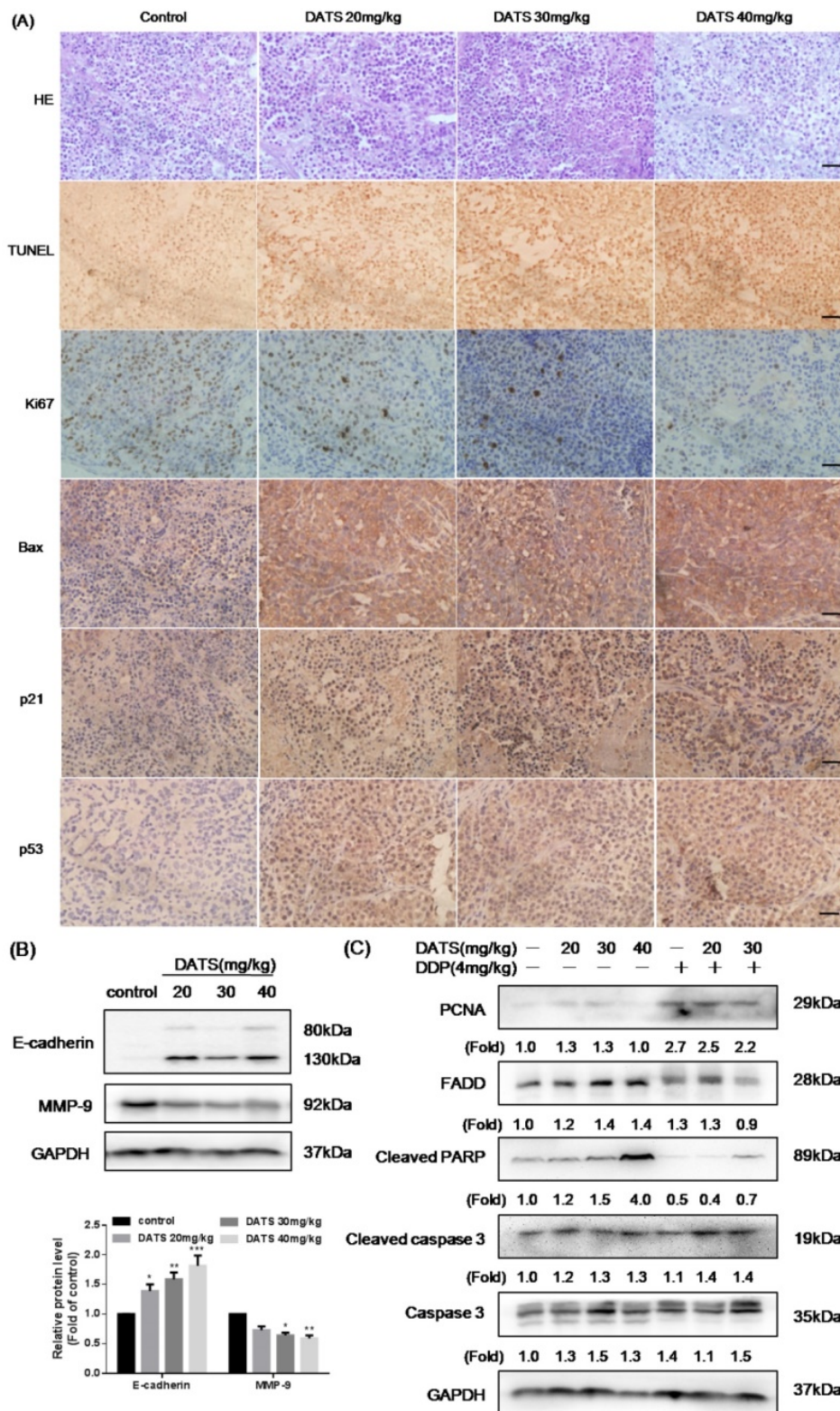


**Figure 5. DATS induced apoptosis in tumor xenografts via activation caspase pathway. (A)** Representative micrographs of tumor sections: hematoxylin and eosin (H&E) staining, TUNEL staining and immunohistochemistry (IHC) for Ki-67, Bax, p21 and p53. Magnification  $\times 400$ , Scale bar = 20  $\mu\text{m}$ . **(B)** Effect of DATS on expression of MMP-9 and E-cadherin,  $*p < 0.05$ ,  $**p < 0.01$ ,  $***p < 0.001$  vs control group. **(C)** Western blot analysis of apoptosis markers, such as PCNA, FADD, cleaved PARP and cleaved caspase-3. The induction fold of proteins was calculated as the intensity of the treatment relative to that of control by densitometry.

### Downregulation of MMP-9 and upregulation of E-cadherin in DATS-treated tumor

Tumor metastasis was the major cause of cancer-related death. The expression of matrix metalloproteinases (MMPs), such as MMP-9, had been implicated in the invasion and metastasis of cancer cells [24]. Besides, the aberrant expression of E-cadherin was a common event in primary invasive carcinomas that progressed to develop distant metastases [25]. Therefore, we performed the formation of MMP-9 and E-cadherin by western blotting to identify the effect of DATS in migration and invasion. Our data showed that DATS increased expression of E-cadherin, and decreased expression of MMP-9, contributing to inhibition of mesenchymal transition (EMT) process (Fig 5B).

### DATS ameliorated Cisplatin-induced oxidative injury in mice bearing tumor

After mice sacrificed, the major organs indexes (liver, kidney and spleen) of mice in each group were also monitored to evaluate the systemic toxicity at the end of treatment. As shown in Fig 6B, DDP

administration alone caused a significant reduction in spleen index, which indicated immune function suppression. While DDP in combined with DATS administration was against the loss in spleen index, which indicated DATS might modulate immune function to prevent body damage.

In addition, kidney index also occurred some changes in DATS groups and combination groups, we further investigated the toxicity of DATS alone and DATS+DDP groups by histopathological examination (for kidney). Light microscopic examination of renal parenchyma revealed normal corpuscular and tubular structures in control and DATS-treated groups. However, in DDP-treated mice, glomerular congestion and atrophy, luminal dilation with excessive accumulation of homogenous casts and mononuclear cells infiltration were observed, which indicated kidney injury. In DDP+DATS treated mice, mild glomerular congestion and inflammatory cell infiltration were observed in the renal parenchyma (Fig 6C). Therefore, DATS could ameliorate DDP-induced kidney injury in mice.

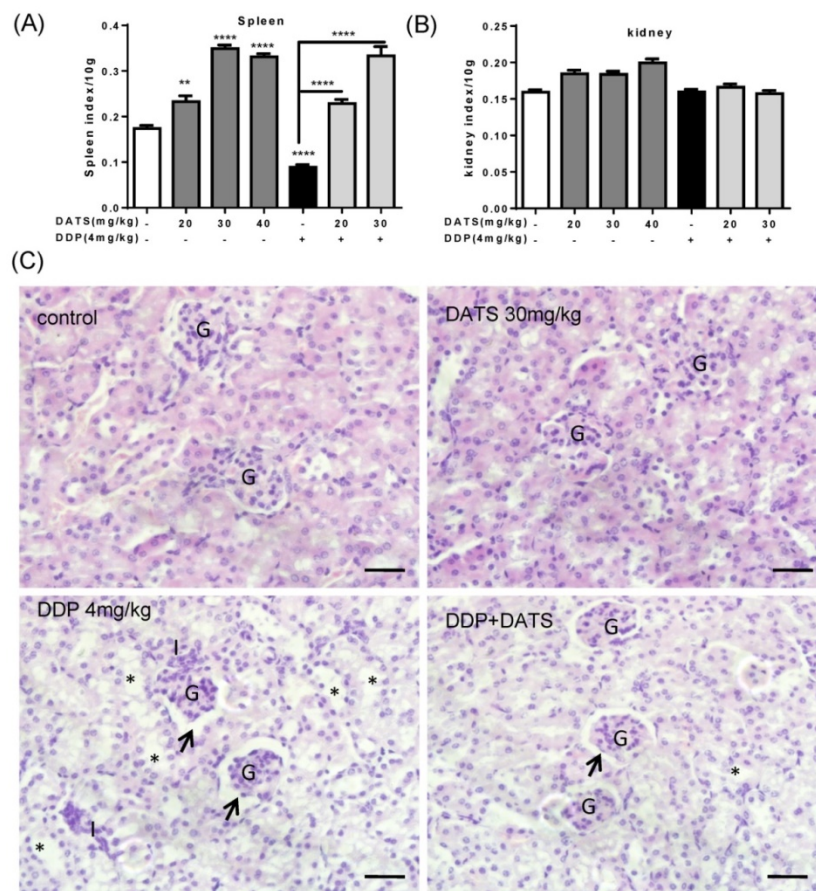


**Figure 6. The toxicity of DATS and combined with DDP in treatment of mice bearing NCI-H460 tumor (A and B)** The changes of major organ (spleen and kidney) indexes of mice at the end of treatment. \* $p < 0.05$ , \*\* $p < 0.01$ , \*\*\* $p < 0.001$ . **(C)** Histological analysis of kidney, original magnification, 400 $\times$ , and scale bar is 20 $\mu$ m. Normal cortical structure is observed in the renal sections of both control and DATS-treated mice. Glomerular atrophy (G), wide capsular space (arrow), wide lumina (\*) with accumulation of homogenous hyaline casts and interstitium inflammatory cell infiltration (I) are noticed in DDP-treated mice. Wide capsular lumina (arrow) and wide lumina (\*) are seen in the combined DATS- and DDP-treated mice.

### DATS modulated the activities of MAPK signal pathway

MAPK pathway has received increasing attention as a target molecule for cancer prevention and therapy. The MAPK cascades include extracellular signal-regulated protei kinases (ERKs), c-Jun N-terminal kinases/stress-activated protein kinases (JNKs/SAPKs), and p38 kinases [26]. To explore the mechanisms underlying the antitumor activity of DATS, we tested the effect of DATS on the activities of PI3K/Akt, MAPK/ERK, MAPK/JNK and MAPK/p38 pathways, which played an important role in cell proliferation, metastasis and survival in cancer. As shown in Fig 7, DATS significantly inhibited phosphorylation of ERK in a dose-dependent manner, Moreover, we found that DATS enhanced phosphorylation of JNK and p38 in these tumor tissues, and promoting effect of DATS on phosphorylation of p38 was dose-dependent. However, we did not find the significant effect of DATS on phosphorylation of Akt. And the combination DDP and DATS inhibited phosphorylation of ERK and p38 compared with DDP alone. These data showed that DATS inhibited the

activity of MAPK/ERK pathway, and activated the MAPK/JNK and MAPK/p38 pathways.

### Discussion

Diallyl trisulfide (DATS), one of the major organosulfur compounds of garlic, has been recognized to have significant antioxidant, antiproliferative and anticarcinogenic properties. Recent studies *in vivo* have found that administration of DATS could inhibit the growth of glioblastoma U87MG [27], human lung A549 tumors [28], human prostate PC-3 tumors [29] and human colon HT-29 tumor [30]. Although anti-cancer effects of DATS on lung cancer cells have been demonstrated [31], there was no information about the effect of DATS alone or combination with other chemotherapeutic agents on NCI-H460 tumors. Nowadays, drug combination attracted great attention due to the advantage of enhanced anti-cancer effects, less drug dose, reduced side effects, etc. In this study, we verify the anticancer effect of DATS on NCI-H460 cells *in vitro* and *in vivo*; focus on whether DATS exerts the enhanced-efficacy of DDP and prevention from its side effect in lung carcinoma treatment.

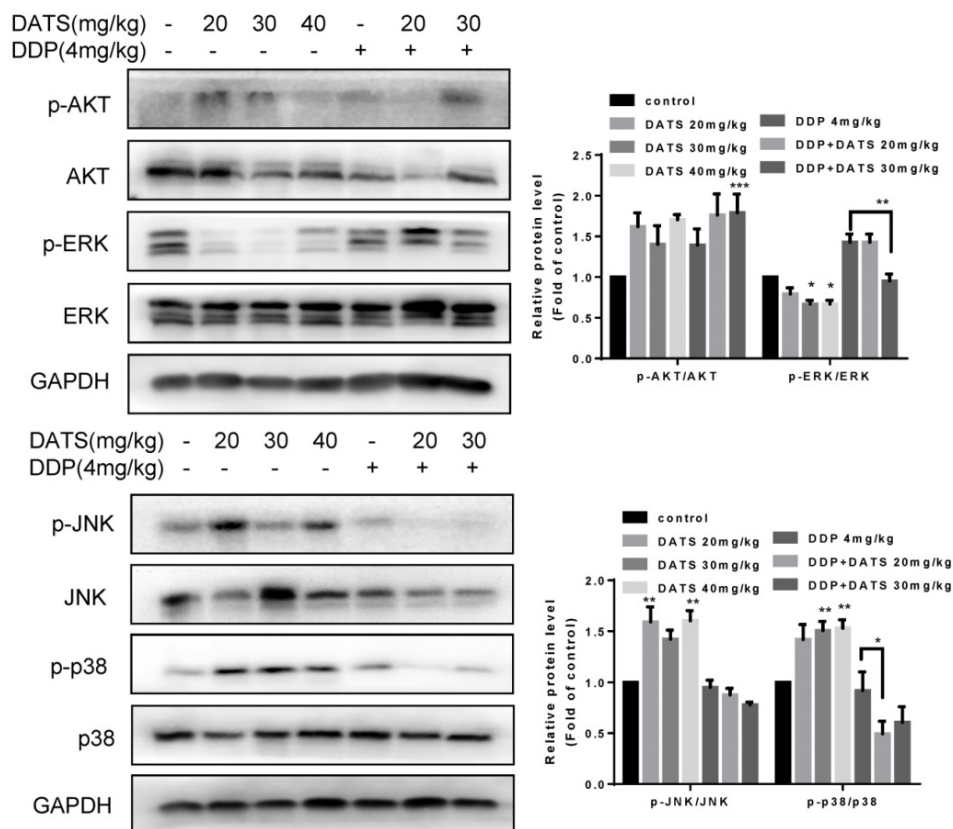


**Figure 7. Modulation of intracellular signaling molecules involved in inflammatory and apoptosis in NCI-H460 tumor tissues.** Effect of DATS on expression of phosphorylated and total Akt, ERK1/2, JNK and p38. The data are presented as the mean ± SEM (n=3), \*p<0.05 and \*\*p<0.01.

The infinite cell proliferation contributes to tumors generation, therefore, induction of cell cycle arrest has been appreciated as a target for cancer treatment [32]. Our results show that DATS exerted anti-proliferative effects in NCI-H460 cells by stabilizing the cell cycle at G<sub>1</sub> phase in association with reduced intracellular levels of cyclin A and B (G<sub>2</sub>/M phase) [33] and increased levels of cyclin D and E (G<sub>1</sub> phase) [34]. These cyclins were believed to indicate the progression of cell cycle and its inactivation leads to cell cycle arrest. DATS also exerted pro-apoptotic properties in a caspase-dependent way through intrinsic and extrinsic pathways. Among the pro-apoptotic factors studied, cytochrome C was also a crucial mediator of the pathway, as it led to the activation of a complex (apoptosome) of caspase-9 and caspase-3 [35]. It is well-known that caspase-3 and caspase-7 catalyzed the processing of native PARP to the active form [36]. Besides, cleaved PARP and caspase-3, the markers of apoptosis, led to the intrinsic apoptosis [37]. The extrinsic pathway of the apoptosis of NCI-H460 cells after the DATS treatment was revealed by the increase of FADD (fas) [38] and the activation of caspase-8 [39]. In addition, p53-mediated pathway was one of the major mechanisms to induce cell death for cancer treatments [40]. It was demonstrated that upregulation of p53 was linked to its downstream target molecule p21 and regulation of the Bcl-2 family members [41]. Our results indicated that the pro-apoptotic factor Bax tended to be upregulated and the pro-survival members (bcl-xL and bcl-2) were reduced by the DATS treatment. These results above demonstrated that DATS exerted excellent anti-proliferative activities, could significantly induce cell cycle arrest and cell apoptosis in NCI-H460 cells.

Furthermore, we investigated the anti-tumor activity of DATS in NCI-H460 xenograft model, and results showed that administration of DATS by daily intraperitoneal injections inhibited the growth of NCI-H460 tumor xenografts without any apparent sign of toxicity in the mice. These results were in accordance with the decreased proliferation documented by Ki67, bax, p21 and p53 immunostaining. DATS induced apoptosis as indicated by TUNEL staining in tumor tissues, at least in part, by activating Bcl-2 family and caspases apoptotic pathways. Additionally, mitogen-activated protein kinases (MAPKs) played major roles in tumor suppression. In this study, we found that treating NCI-H460 lung cancer tumor with DATS changed the levels of all three pathways in MAPKs. Surprisingly, JNK and p38 activation were involved in DATS-mediated tumor inhibition. Considerable evidences suggested activation of JNK pathway

induced mitochondria-dependent cell apoptosis via activating mitochondrial Bcl-2 family proteins [42]. Activation of p38 MAPK was often accompanied by activation of caspase-3 [43], which then induced the apoptotic caspase cascade. Besides, tumor metastasis was the major cause of cancer-related death, and our data showed DATS-mediated tumor metastasis inhibition was accompanied by increased E-cadherin and decreased MMP-9 expressions. These *in vivo* results were consistent with our studies *in vitro*, which further suggested that DATS may be an applicable approach to enhance the antitumor activity against lung cancer.

Based on the facts that DATS administration caused body weight increase, we conducted a study of combining DDP with DATS to act on female BALB/c nude mice bearing NCI-H460 xenograft tumor and found that combined administration enhanced the inhibition of xenograft tumor growth and attenuated the DDP-mediated weight loss. DDP+DATS increased the expression of cleaved caspase-3 and cleaved PARP compared with DDP alone, which contributed to tumor apoptosis process. In addition, we observed the increased spleen index in DATS treatment group, which suggested that DATS could enhance immune response. Besides, DATS could attenuate the disorder of renal parenchyma induced by DDP and provide protection from oxidative injury in tumor treatment.

In summary, the current study demonstrated that DATS exhibits antitumor activity in human lung carcinomas NCI-H460 cells both *in vitro* and *in vivo*; and DATS in combination with DDP exerts promising synergistic activities with fewer adverse effects in nude mice. Thus combining DATS with DDP may provide a novel therapeutic strategy for further clinical development in cancer treatment.

## Acknowledgements

This work was supported by the funds from National “Major Science and Technology Project-Prevention and Treatment of AIDS, Viral Hepatitis, and Other Major Infectious Diseases” (Grant #2013ZX10005004), Major Project of Science and Technology of Shandong Province (Grant #2015ZDJS04001), Science & Technology Enterprise Technology Innovation Fund of Jiangsu Province (Grant #BC2014172), Small & Medium Enterprise Technology Innovation Project of Lianyungang City (Grant #CK1333).

## Competing Interests

The authors have declared that no competing interest exists.

## References

- Ozkok A, Edelstein CL. Pathophysiology of cisplatin-induced acute kidney injury. *Biomed Research International*. 2014; 2014: 1209-15.
- Jin ZY, Wu M, Han RQ, Zhang XF, Wang XS, Liu AM, et al. Raw garlic consumption as a protective factor for lung cancer, a population-based case-control study in a Chinese population. *Cancer Prevention Research*. 2013; 6.
- Myneni AA, Chang SC, Niu R, Liu L, Swanson MK, Li J, et al. Raw garlic consumption and lung cancer in a Chinese population. *Cancer Epidemiology Biomarkers & Prevention*. 2016.
- Katsuki T, Hirata K, Ishikawa H, Matsuura N, Sumi SI, Itoh H. Significance of Garlic and Its Constituents in Cancer and Cardiovascular Disease. *Journal of the American Academy of Dermatology*. 1997; 36: S1-S2.
- Sun X, Guo T, He J, Zhao M, Yan M, Cui F, et al. Determination of the concentration of diallyl trisulfide in rat whole blood using gas chromatography with electron-capture detection and identification of its major metabolite with gas chromatography mass spectrometry. *Yakugaku Zasshi Journal of the Pharmaceutical Society of Japan*. 2006; 126: 521-7.
- Germain E, Auger J, Ginies C, Siess MH, Teyssier C. In vivo metabolism of diallyl disulphide in the rat: identification of two new metabolites. *Xenobiotica*. 2003; 32: 1127-38.
- Lai KC, Hsu SC, Kuo CL, Yang JS, Ma CY, Lu HF, et al. Diallyl sulfide, diallyl disulfide, and diallyl trisulfide inhibit migration and invasion in human colon cancer colo 205 cells through the inhibition of matrix metalloproteinase-2, -7, and -9 expressions. *Environmental Toxicology*. 2013; 28: 479-88.
- Na HK, Kim EH, Choi MA, Park JM, Kim DH, Surh YJ. Diallyl trisulfide induces apoptosis in human breast cancer cells through ROS-mediated activation of JNK and AP-1. *Biochemical Pharmacology*. 2012; 84: 1241-50.
- Powolny AA, Singh SV. Multitargeted prevention and therapy of cancer by diallyl trisulfide and related Allium vegetable-derived organosulfur compounds. *Cancer Letters*. 2008; 269: 305-14.
- Antony ML, Singh SV. Molecular mechanisms and targets of cancer chemoprevention by garlic-derived bioactive compound diallyl trisulfide. *Indian Journal of Experimental Biology*. 2011; 49: 805-16.
- Xian HX, Gai LL, Bing AW, Yang Q, Shu RB, Jian R, et al. Diallyl trisulfide protects against oxygen glucose deprivation -induced apoptosis by scavenging free radicals via the PI3K/Akt -mediated Nrf2/HO-1 signaling pathway in B35 neural cells. *Brain Research*. 2015; 1614: 38-50.
- You S, Nakanishi E, Kuwata H, et al. Inhibitory effects and molecular mechanisms of garlic organosulfur compounds on the production of inflammatory mediators. *Molecular Nutrition & Food Research*. 2013; 57: 2049-60.
- Tsai CY, Wang CC, Lai TY, Tsu HN, Wang CH, Liang HY, et al. Antioxidant effects of diallyl trisulfide on high glucose-induced apoptosis are mediated by the PI3K/Akt-dependent activation of Nrf2 in cardiomyocytes. *International Journal of Cardiology*. 2013; 168: 1286-97.
- Kyo E, Uda N, Suzuki A, Kakimoto M, Ushijima M, Kasuga S, et al. Immunomodulation and antitumor activities of Aged Garlic Extract. *Phytomedicine International Journal of Phytotherapy & Phytomedicine*. 1998; 5: 259-67.
- Lamm DL, Riggs DR. Enhanced immunocompetence by garlic: role in bladder cancer and other malignancies. *Journal of Nutrition*. 2001; 131: 1067S-70S.
- Kyo E, Uda NS, Itakura Y. Immunomodulatory effects of aged garlic extract. *Journal of Nutrition*. 2001; 131: 1075-9.
- Ebrahimpour S, Tabari MA, Youssefi MR, Aghajanzadeh H, Behzadi MY. Synergistic effect of aged garlic extract and naltrexone on improving immune responses to experimentally induced fibrosarcoma tumor in BALB/c mice. *Pharmacognosy Research*. 2013; 5: 189-94.
- Alkreaty HM, Damanhouri ZA, Ahmed N, Slevin M, Osman AM. Mechanisms of cardioprotective effect of aged garlic extract against Doxorubicin-induced cardiotoxicity. *Integrative Cancer Therapies*. 2012; 11: 364-70.
- Rafieian-Kopaei M, Baradaran A, Merrikhi A, Nematbakhsh M, Madihi Y, Nasri H. Efficacy of Co-administration of Garlic Extract and Metformin for Prevention of Gentamicin-Renal Toxicity in Wistar Rats: A Biochemical Study. *International Journal of Preventive Medicine*. 2013; 4: 258-64.
- Hydbring P, Malumbres M, Sicinski P. Non-canonical functions of cell cycle cyclins and cyclin-dependent kinases. *Nature Reviews Molecular Cell Biology*. 2016.
- Takita M, Furuya T, Sugita T, Kawachi S, Oga A, Hirano T, et al. An analysis of changes in the expression of cyclins A and B1 by the cell array system during the cell cycle: Comparison between cell synchronization methods. *Cytometry Part A*. 2003; 55A: 24-9.
- Yip KW, Reed JC. Bcl-2 family proteins and cancer. *Oncogene*. 2008; 27: 6398-406.
- Olsson M, Zhivotovsky B. Caspases and cancer. *Cell Death & Differentiation*. 2011; 18: 1441-9.
- Deryugina EI, Quigley JP. Matrix metalloproteinases and tumor metastasis. *Cancer & Metastasis Reviews*. 2006; 25: 9-34.
- Bremnes RM, Veve R, Hirsch FR, Franklin WA. The E-cadherin cell-cell adhesion complex and lung cancer invasion, metastasis, and prognosis. *Lung Cancer*. 2002; 36: 115-24.
- Kyriakis JM, Avruch J. Mammalian MAPK signal transduction pathways activated by stress and inflammation: a 10-year update. *Physiological Reviews*. 2012; 92: 689-737.
- Iv GCW, Haar CP, Iii WAV, Giglio P, Dixon-Mah YN, Varma AK, et al. Multi-targeted DATS prevents tumor progression and promotes apoptosis in ectopic glioblastoma xenografts in SCID mice via HDAC inhibition. *Journal of Neuro-Oncology*. 2013; 114: 43-50.
- Wenjun, Tian, Shuhai, Weiming, Zhitao, Chen, et al. Diallyl trisulfide induces apoptosis and inhibits proliferation of A549 cells in vitro and in vivo. *Acta Biochimica Et Biophysica Sinica*. 2012; 44: 577-83.
- Xiao D, Lew KL, Kim YA, Zeng Y, Hahm ER, Dhir R, et al. Diallyl trisulfide suppresses growth of PC-3 human prostate cancer xenograft in vivo in association with Bax and Bak induction. *Clinical Cancer Research An Official Journal of the American Association for Cancer Research*. 2006; 12: 6836-43.
- Lai KC, Hsu SC, Yang JS, Yu CC, Lein JC, Chung JG. Diallyl trisulfide inhibits migration, invasion and angiogenesis of human colon cancer HT-29 cells and umbilical vein endothelial cells, and suppresses murine xenograft tumour growth. *Journal of Cellular & Molecular Medicine*. 2015; 19: 474-84.
- Xiao D, Zeng Y, Hahm ER, Kim Y, Ramalingam S, Singh SV. Diallyl trisulfide selectively causes Bax-and Bak-mediated apoptosis in human lung cancer cells. *Environmental and molecular mutagenesis*. 2009; 50: 201-12.
- T W, Y Z, L D, J Y, K K, B V, et al. Cell-cycle arrest versus cell death in cancer therapy. *Nature Medicine*. 1997; 3: 1034-6.
- C B, J B, J S-T, H H, M C, M J, et al. p53-dependent G2 arrest associated with a decrease in cyclins A2 and B1 levels in a human carcinoma cell line. *British Journal of Cancer*. 2000; 82: 642-50.
- Baldin V, Lukas J, Marcote MJ, Pagano M, Draetta G. Cyclin-D1 is a nuclear protein required for cell cycle progression G1. *Genes & Development*. 1993; 7: 812-21.
- Li P, Nijhawan D, Budihardjo I, Srinivasula SM, Ahmad M, Alnemri ES, et al. Cytochrome c and dATP-dependent formation of Apaf-1/caspase-9 complex initiates an apoptotic protease cascade. *Cell*. 1997; 91: 479-89.
- Los M, Mozoluk M, Ferrari D, Stepczynska A, Stroch C, Renz A, et al. Activation and caspase-mediated inhibition of PARP: a molecular switch between fibroblast necrosis and apoptosis in death receptor signaling. *Molecular biology of the cell*. 2002; 13: 978-88.
- Boulares AH, Yakovlev AG, Ivanova V, Stoica BA, Wang G, Iyer S, et al. Role of poly (ADP-ribose) polymerase (PARP) cleavage in apoptosis Caspase 3-resistant PARP mutant increases rates of apoptosis in transfected cells. *Journal of Biological Chemistry*. 1999; 274: 22932-40.
- Lee EW, Seo J, Jeong M, Lee S, Song J. The roles of FADD in extrinsic apoptosis and necroptosis. *Biochemistry & Molecular Biology Reports*. 2012; 45: 496-508.
- Jin Z, Li Y, Pitti R, Lawrence D, Pham VC, Lill JR, et al. Cullin3-Based Polyubiquitination and p62-Dependent Aggregation of Caspase-8 Mediate Extrinsic Apoptosis Signaling. *Cell*. 2009; 137: 721-35.
- Pietenpol JA, Stewart ZA. Cell cycle checkpoint signaling: Cell cycle arrest versus apoptosis. *Toxicology*. 2002; 181-182: 475-81.
- Lee D-H, Ha J-H, Kim Y, Jang M, Park SJ, Yoon HS, et al. A conserved mechanism for binding of p53 DNA-binding domain and anti-apoptotic Bcl-2 family proteins. *Molecules and cells*. 2014; 37: 264-9.
- Wei Y, Sinha SC, Levine B. Dual role of JNK1-mediated phosphorylation of Bcl-2 in autophagy and apoptosis regulation. *Autophagy*. 2008; 4: 949-51.
- Zhuang S, Demirs JT, Kochevar IE. p38 mitogen-activated protein kinase mediates bid cleavage, mitochondrial dysfunction, and caspase-3 activation during apoptosis induced by singlet oxygen but not by hydrogen peroxide. *Journal of Biological Chemistry*. 2000; 275: 25939-48.